

REVERSE BEND OPTION FOR A 6 GeV STORAGE RING LATTICE

L. Houmami*, N. Carmignani, L.R. Carver, F. Cianciosi, S.M. Liuzzo, T. Perron, S. White, ESRF, Grenoble, France

Abstract

Several high-energy synchrotron facilities adopted the Hybrid Multi-Bend Achromat scheme (HMBA) developed for the ESRF-EBS [1]. The considered lattice has been developed for a generic 6 GeV storage ring (SR) of 1100 m circumference [2]. It includes a short bending (SB) magnet at the center of the cell, and achieves a ~ 70 pm rad equilibrium horizontal emittance. The optics of such SR are modified introducing reverse bending magnets [3,4] to further reduce the natural horizontal emittance to 53 pm rad. The impact of such modification on dynamic aperture and lifetime is assessed and optimized.

INTRODUCTION

The present work has been developed for a generic high-energy storage ring of 6 GeV and 1100 m circumference [2]. The lattice considered is an adaptation of the ESRF-EBS H7BA lattice [5] with 40 cells, achieving ~ 70 pm rad horizontal emittance. Figure 1 displays the optics of a standard cell of the presented ring.

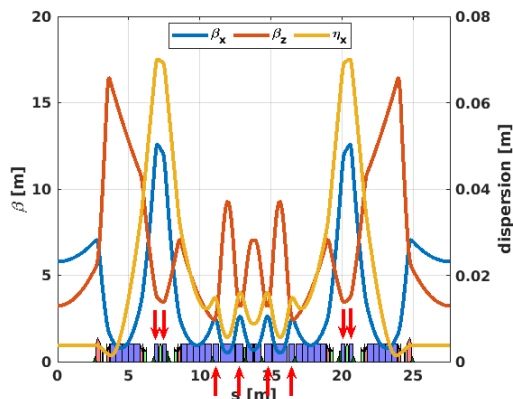


Figure 1: Location of the reverse bends (red arrows) in the lattice. All dipoles are represented in blue.

Further reduction of the horizontal emittance is achievable with a fixed lattice layout, by controlling the dispersion function at the entrance of the dipole magnets, to approach the Theoretical Minimum Emittance (TME) conditions [6]. Reverse bends (RB), which are mechanically displaced quadrupoles with regards to the machine axis, generate a negative dipolar field of resulting angle [4]:

$$\theta^{RB} = -k_1 l \Delta x \quad (1)$$

with k_1 the strength of the quadrupole, l its length and Δx the horizontal displacement. Such quadrupoles help modulate the dispersion function and derivative to approach the TME

* lina.houmami@esrf.fr

in the dipoles [3]. Previous attempts were conducted on a similar lattice [7].

ANGULAR CORRECTION

All focusing quadrupoles in the dispersive area were used as reverse bends to optimise the emittance reduction. Their location is displayed in Fig. 1. The introduction of negative angles perturbs both the geometry and the dispersion in the standard cell, reducing the total angle per cell. The correction of the total angle is pursued using two methods:

- **Transposed method** The total reverse bending angle per cell θ_{tot}^{RB} is defined as the sum of all negative bending angles, expressed per RB in Eq. 1. It is compensated by shifting the standard dipole angles to recover the geometry of the cell. The angular distribution along the cell simply becomes $\theta^{RB} = -\frac{|\theta_{tot}^{RB}|}{N_{RB}}$ for RB and $\theta_{dip} = \theta_0 + \frac{|\theta_{tot}^{RB}|}{N_{dip}}$ for the standard bending magnets, where N_{RB} , N_{dip} are respectively the number of RB and dipoles in the cell, and θ_0 the bending angle of the dipoles in the nominal lattice.
- **Proportional method** The total angle is restored proportionally over the whole cell, applying the following operation on all bending magnets: $\theta_{new} = \frac{2\pi\theta_{old}}{N_{cells}*a}$, where a is the cell angle before correction, and N_{cells} the number of cells of the machine. This method conserves the perturbation of the dispersion of the reverse bends, for which we expect a stronger emittance reduction.

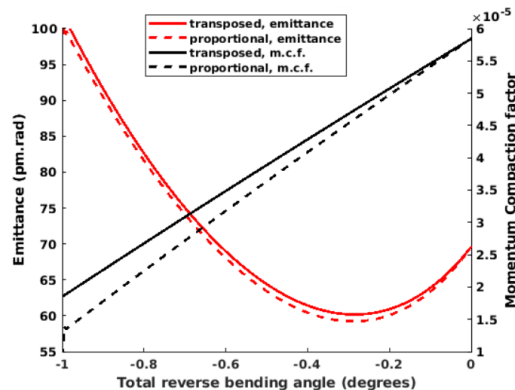


Figure 2: Evolution of the emittance and the momentum compaction factor (m.c.f.) with the total reverse bending angle, for the two methods of angle restoration.

Both methods were tested and compared in Accelerator Toolbox (A.T.) [8], for different total reverse bending angles

θ_{tot}^{RB} . To ease the comparison, θ_{tot}^{RB} was equally distributed among the reverse bends. As the dispersion is perturbed by the insertion of the reverse bends and by the correction of the total angle, the lattice optics are rematched at each step in θ_{tot}^{RB} . Figure 2 superimposes the variation of the emittance and momentum compaction factor with θ_{tot}^{RB} for both methods considered. Table 1 compares the main characteristics of the lattices without and with reverse bends at the minimum emittance generated with the two methods detailed above. The smallest natural horizontal emittance (59 pm rad) is achieved with the proportional method, with similar total reverse bending angle and energy spread, and lower radiation losses.

Table 1: Comparison of Main Standard Cell Parameters for the Two Lattices with Reverse Bends of Minimum Natural Horizontal Emittance Obtained with Two Methods of Angular Correction

| Parameter | Nominal | Method | |
|-------------------------------|--------------------|--------------------|----------------------|
| | | Transposed | Proport. |
| θ_{tot}^{RB} (degrees) | 0 | -0.27 | -0.29 |
| ϵ_x (pm.rad) | 70.0 | 66.9 | 59.2 |
| σ_E | 9×10^{-4} | 10^{-3} | 10^{-3} |
| m.c.f. | 6×10^{-5} | 5×10^{-5} | 4.5×10^{-5} |
| J_x | 1.54970 | 1.91472 | 1.93536 |
| Radiation loss | 50 keV | 56 keV | 54 keV |

OPTIMISATION OF THE REVERSE BENDING ANGLE DISTRIBUTION

To find the lowest horizontal natural emittance, the reverse bends are freely varied, conserving the proportional method for angular correction. Four knobs, respecting the cell axial symmetry, are used to seek for the minimum horizontal emittance. The inhomogeneous angular distribution frees the total reverse bending angle θ_{tot}^{RB} , which optimum was previously limited to the parabolic evolution of the \mathcal{H} -function with the dispersion functions. The total reverse bending angle is varied by ± 0.01 degrees between consecutive iterations of a minimization process.

Each iteration randomly generates five angular distributions in the reverse bends. For each of these distributions the total angle is corrected with the proportional method and the optics are matched. For a given θ_{tot}^{RB} , the distribution of minimum emittance is chosen. This ring is then reintroduced as the input of the next scan. The scan controls the horizontal damping partition number for sake of longitudinal stability.

The variation of both the horizontal natural emittance and the momentum compaction factor during the conducted scans are displayed in Fig. 3. The natural horizontal emittance first follows a parabolic variation with θ_{tot}^{RB} and then the inhomogeneous distribution of the reverse angles allows

the increase of θ_{tot}^{RB} , further reducing the emittance. The optimisation is stopped at -0.5 degrees after convergence.

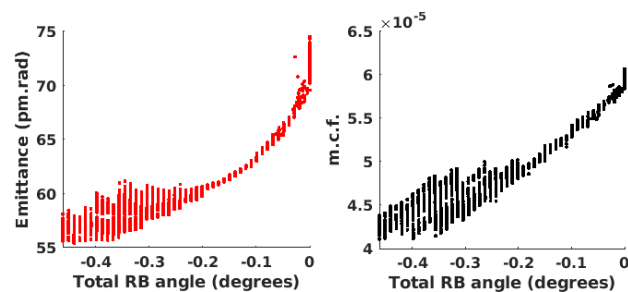


Figure 3: Variation of (left) the natural horizontal emittance and (right) the momentum compaction factor during the cycle of the algorithm. The large number of points per angle originates from the random reverse-angle distribution and the two-sided evolution of the total reverse bending angle θ_{tot}^{RB} .

LATTICE OPTION WITH 53.1 pm rad EMITTANCE

After selection of the optimum standard cell option using the previous scan, high- β_x injection cells are matched to the ESRF-EBS ones [5]. The standard cells reverse bends were included in the injection cells, to close the ring geometry. The circumference of the ring was increased to set the harmonic number to 1296, for a RF frequency of 352.2 MHz [9]. Control of the dispersion at the middle of the standard cell allowed a total reduction in horizontal emittance to about 53 pm rad for the ring with reverse bends. Main parameters are listed for the lattices with and without reverse bends in Table 2.

Table 2: Comparison of Main Parameters for the Nominal Lattice and its Option with Reverse Bends

| Parameter | Nominal | RB option |
|--|----------------------|----------------------|
| Circumference | 1100 m | 1103 m |
| (Q_x, Q_y) | (95.21, 33.34) | (95.21, 34.34) |
| ϵ_x (pm.rad) | 70.0 | 53.1 |
| θ_{tot}^{RB} (degrees) per cell | 0 | -0.35 |
| σ_E | 8.6×10^{-4} | 1.0×10^{-3} |
| m.c.f. | 6×10^{-5} | 5×10^{-5} |
| Energy loss | 2.0 MV | 2.2 MV |
| Chromaticity | (7,6) | (1,5) |
| RF Frequency | 352.0 MHz | 352.2 MHz |
| Harmonic number | 1294 | 1296 |
| Nat. bunch length | 2.9 mm | 3.4 mm |

Table 3 lists the characteristics of the reverse bending magnets and their corresponding horizontal shift. The main contribution in the emittance reduction comes from the central part of the lattice (between 11 and 17 m in Fig. 1), with a

maximum 2.1 mm shift required. To compare, the maximum transverse displacement values Δx_{max} in the ESRF-EBS are determined by analysis of the full cell assembly drawings and are reduced by about 1 mm considering the presence of kapton foils under the dispersion bump and the vacuum chambers, and specific vacuum chambers shapes and positioning of heating wires for the central reverse bends [10]. The displacement of high-gradient quadrupoles exceeds the maximum available. Vacuum chambers may need specific design adjustments compared to those of EBS.

Table 3: Horizontal Shifts Δx of the Implemented Reverse Bends

| Name | QF4[AE] | QF4[BD] | QF6 | QF8 |
|--------------------------|---------|---------|---------|---------|
| Length (m) | 0.21 | 0.21 | 0.39 | 0.48 |
| k_2 (m ⁻²) | 2.6 | 2.2 | 4.52 | 4.42 |
| Δx (mm) | 0.18 | 0.29 | 2.1 | 1.9 |
| Δx_{max} (mm) | 2.4-3.4 | 2.4-3.4 | 1.2-2.2 | 1.2-2.2 |

DYNAMIC APERTURE AND LIFETIME

Optimisation of the sextupoles started with a scan of the ring chromaticity to optimise both the Touschek lifetime (TL) and the transverse dynamic aperture. Particles were tracked for 2000 turns and the momentum acceptance was computed over four standard cells for computing time considerations. The Touschek lifetime was calculated assuming the same uniform filling pattern as ESRF-EBS, 200 mA in 1296 bunches [11]. Figure 4 gathers the resulting dynamic aperture area and the Touschek lifetime for the scanned chromaticities. The best compromise found between Touschek lifetime at high current and on-momentum dynamic aperture at the injection point was found for the chromaticity (1,5).

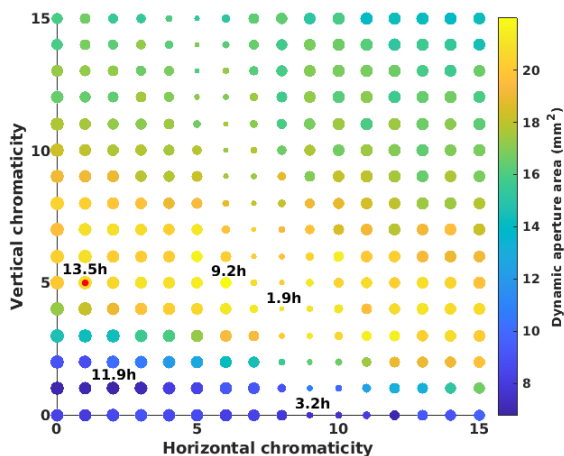


Figure 4: Touschek lifetime (dot size) and dynamic aperture area (color) variation with chromaticity for the H7BA ring with reverse bends, for $Z_N = 0.67 \Omega$ and $\epsilon_V = 10$ pm rad. The maximum TL and DA were obtained for a chromaticity (1,5) (red dot).

Figure 5 compares the dynamic aperture (DA) of the nominal lattice and its option with reverse bends of chromaticity (1,5) with high-beta injection cells to increase the dynamic aperture at injection. Particles are tracked starting at the injection point for 5000 turns. The standard cell with reverse bends presents a reduction of its dynamic aperture which remains comparable to the nominal one. The high- β_x injection cells improve the horizontal transverse acceptance at injection for the lattice without reverse bends as expected, but not for the lattice with RB. Their impact on the lifetime is also detrimental on the Touschek lifetime: when the 40-fold symmetry ring with reverse bends presents a 32 h lifetime for 200 mA in 1296 bunches, the insertion of the injection cells with reverse bends reduce it to 13.5 h. Tuning of the injection is therefore mandatory to enhance the DA at injection point, with less impact on the Touschek lifetime.

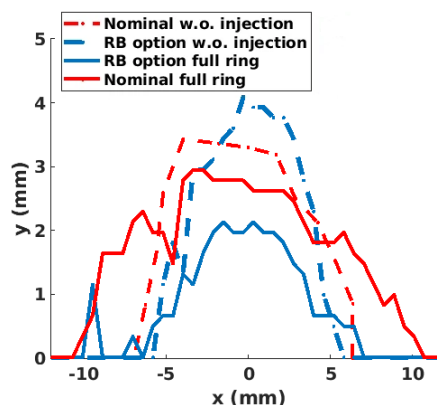


Figure 5: Dynamic aperture of the standard cell (dots) and ring with injection cells (plain) for the lattices with (black) and without (red) reverse bends.

CONCLUSION

A H7BA lattice for a 6 GeV 1100 m storage ring was presented, with a 70 pm rad natural horizontal emittance. Further reduction of its emittance can be achieved with reverse bending magnets with no additional constraint to the optics. The angle correction procedure was discussed. The proportional correction was selected for it achieved lower emittance and lower radiation losses.

Further optimisation of the reverse bending angle distribution was achieved in A.T., by tuning four RB knobs. A minimum emittance of 53 pm rad was achieved with this algorithm while conserving horizontal shifts at the limit of feasibility for each magnet. The full ring includes high- β_x injection cells like for ESRF-EBS. Nonetheless, the dynamic aperture was not increased at the injection point and a reduction of about 20 h in Touschek lifetime was calculated. Further studies will focus on upgrading the injection cells in terms of optics and optimising the injection sextupoles to restore the high dynamic aperture and reduce their detrimental effect on the beam lifetime.

REFERENCES

- [1] L. Farvacque *et al.*, “A Low-Emittance Lattice for the ESRF”, in *Proc. IPAC’13*, Shanghai, China, May 2013, paper MO-PEA008, pp. 79–81.
- [2] S. M. Liuzzo *et al.*, “USSR HMBA Storage Ring Lattice Options”, in *Proc. IPAC’21*, Campinas, Brazil, May 2021, pp. 1466–1469. doi:10.18429/JACoW-IPAC2021-TUPAB049
- [3] A. Streun *et al.*, “The anti-bend cell for ultralow emittance storage ring lattices”, *Nucl. Instrum. Methods Phys. Res., Sect. A*, vol. 137, pp. 148-154, 2014. doi:10.1016/j.nima.2013.11.064
- [4] B. Riemann and A. Streun, “Low emittance lattice design from first principles: Reverse bending and longitudinal gradient bends”, *Phys. Rev. Accel. Beams*, vol. 22, p. 021601, 2019. doi:10.1103/PhysRevAccelBeams.22.021601
- [5] ESRF Orange book, <https://www.esrf.fr/about/upgrade>
- [6] H. Wiedemann, *Particle Accelerator Physics*, Third edition, Berlin, Germany: Springer, 2007, p. 305.
- [7] V.S. Dyubkov, T. Kulevoy, and E.D. Tsyplakov, “Lattice Options With Reverse Bending Magnets for USSR HMBA Storage Ring”, in *Proc. RuPAC’21*, Alushta, Russia, pp. 280–282, 2021. doi:10.18429/JACoW-RuPAC2021-TUPSB26
- [8] B. Nash *et al.*, “New Functionality for Beam Dynamics in Accelerator Toolbox (AT)”, in *Proc. IPAC’15*, Richmond, VA, USA, May 2015, pp. 113–116. doi:10.18429/JACoW-IPAC2015-MOPWA014
- [9] V. Serriere *et al.*, “352.2 MHz HOM Damped Normal Conducting ESRF Cavity: Design and Fabrication”, in *Proc. IPAC’11*, San Sebastian, Spain, Sep. 2011, paper MOPC004, pp. 68–70.
- [10] EBS Technical Design Report, <https://www.esrf.fr/files/live/sites/www/files/about/upgrade/documentation/Design>
- [11] J.-L. Revol *et al.*, “ESRF-EBS: Implementation, Performance and Restart of User Operation”, in *Proc. IPAC’21*, Campinas, Brazil, May 2021, pp. 3929–3932. doi:10.18429/JACoW-IPAC2021-THPAB074